Development of a platform of 3D adipogenesis to model, at higher scale, the impact of LY2090314 compound on fibro/adipogenic progenitor adipogenic drift

Alessio Reggio[1], Francesca De Paolis[1,2], Salma Bousselmi[1], Felice Cicciarelli[1], Sergio Bernardini[1], Alberto Rainer[3,4], Dror Seliktar[5], Stefano Testa[6], Carmine Cirillo[7], Paolo Grumati[7,8], Stefano Cannata[1], Claudia Fuoco[1,*], Cesare Gargioli[1,*]

[1]Department of Biology, University of Rome "Tor Vergata", Rome, 00133, Italy
[2]PhD Program in Cellular and Molecular Biology, Department of Biology, University of Rome "Tor Vergata", 00133, Rome, Italy
[3]Department of Engineering, Università Campus Bio-Medico, Rome, 00128, Italy
[4]Institute of Nanotechnology (NANOTEC), National Research Council, Lecce, 73100, Italy
[5]Department of Biomedical Engineering, Techion Institute, Haifa, Israel
[6]Aix Marseille University, INSERM, Marseille Medical Genetics, MMG, Marseille, France
[7]Telethon Institute of Genetics and Medicine (TIGEM), Pozzuoli (NA), Italy
[8]Department of Clinical Medicine and Surgery, Federico II University, Naples, Italy

[*]Correspondence: claudia.fuoco@uniroma2.it and cesare.gargioli@uniroma2.it

Summary statement

LY2090314 suppresses 2D and 3D adipogenesis of fibro/adipogenic progenitors by stabilizing a transcriptional competent β-catenin complex.

Abstract

In human dystrophies, the progressive muscle wasting is exacerbated by ectopic deposition of fat and fibrous tissue originating from fibro/adipogenic progenitors (FAPs). In degenerating muscles, the ability of these cells to adjuvate a successful healing is attenuated and FAPs aberrantly expand and differentiate into adipocytes and fibroblasts. Thus, arresting the fibroadipogenic fate of FAPs, without affecting their physiological role, represents a valuable therapeutic strategy for patients affected by muscle diseases. Here, using a panel of adipose progenitor cells including human-derived FAPs coupled with pharmacological perturbations and proteome profiling, we report that LY2090314 interferes with a genuine adipogenic program acting as WNT surrogate for the stabilization of a competent β-catenin transcriptional complex. To predict the beneficial impact of LY2090314 in limiting ectopic deposition of fat in human muscles, we combined the Poly-Ethylene-Glycol-Fibrinogen biomimetic matrix with these progenitor cells to create a

miniaturized 3D model of adipogenesis. Using this scalable system, we demonstrated that a two-digit nanomolar dose of this compound is effective to repress adipogenesis in a higher 3D scale, thus offering a concrete proof for the use of LY2090314 to limit FAP-derived fat infiltrates in dystrophic muscles.

Keywords: Muscular dystrophies, adipogenesis, fibro/adipogenic progenitors, β-catenin, LY2090314, tissue engineering.

Highlights

- LY2090314 is capable of inhibiting adipogenesis of murine and human fibro/adipogenic progenitors, the cell population responsible for fatty degenerative outcomes in diseased skeletal muscles.

- High-resolution proteomics revealed that the anti-adipogenic role of LY2090314 is mediated by a primary mechanism that is ascribed to the role of LY2090314 of inhibiting GSK kinase, and a second indirect mechanism that further strength GSK blockage via WNT5A.

- The coupling of the PEG-Fibrinogen biomimetic matrix with adipose progenitors generates a 3D model of adipogenesis.

- Miniaturized 3D adipogenesis is useful to test candidate antiadipogenic compounds. A single two-digit nanomolar dose of LY2090314 significantly represses adipogenesis in a complex 3D scale.

Introduction

Fibro/adipogenic progenitors (FAPs) are interstitial cells residing in all tissues of mesenchymal origin. Independently from the source, these cells share conserved roles and functions by being primarily devoted to the overall maintenance of tissue homeostasis (Contreras et al., 2021; Giuliani et al., 2021). In skeletal muscle tissue, FAP cells contribute to sustain the regenerative potential and the mass of postnatal muscles by preserving and supporting adult muscle stem cells, namely satellite cells (SCs) (Uezumi et al., 2021; Wosczyna et al., 2019). Regrettably, in degenerating muscles, the ability of FAPs to adjuvate a successful healing is attenuated, and these cells tend to differentiate into adipocytes and fibroblasts, aggravating the clinical portrait of the affected muscles (Madaro et al., 2018; Santini et al., 2020; Uezumi et al., 2011). Ectopic deposition of

adipocytes ruinously exacerbates muscular dystrophies (Emery, 2002), including Duchenne Muscular Dystrophy (DMD), limb girdle muscular dystrophies, Emery-Dreyfuss muscular dystrophy and other myopathies (Bosnakovski et al., 2017; Hogarth et al., 2019; Uezumi et al., 2011; Uezumi et al., 2014). Adipose infiltrates are also common in other diseases such as obesity (Akhmedov and Berdeaux, 2013; Buras et al., 2019; Pérez-Díaz et al., 2022), type II diabetes (Farup et al., 2021), and correlate with muscle wasting during ageing (Volpi et al., 2004).

Pharmacological agents capable to alter FAP adipogenesis have been identified(Cordani et al., 2014; Farup et al., 2021; Kasai et al., 2017; Kopinke et al., 2017; Mozzetta et al., 2013; Reggio et al., 2019; Reggio et al., 2020b), concretizing only recently the possibility to significantly mitigate intramuscular fatty degeneration.

Recently, endogenous WNT ligands are emerging as a critical regulator of FAP behavior, suggesting that the manipulation of WNT pathway components, via small molecules, may represent a feasible strategy for limiting the adipogenic drift of these cells (Reggio et al., 2020b). In the last years, our group uncovered GSK3 kinase as a transducer that controls adipogenesis, while identifying GSK3 inhibitors as valuable candidates to impair FAP adipogenic fate (Reggio et al., 2020b). Specifically, we demonstrated that a short-term exposure to LY2090314, a highly potent GSK3 inhibitor, is capable to limit fatty degeneration in glycerol-degenerating muscles as well as inhibit adipogenesis of FAPs extracted from dystrophic *mdx* muscles (Reggio et al., 2020b).

In the present work, we provide pharmacological evidences that an active β-catenin transcriptional complex intimately represses the adipogenic program of adipose progenitor cells, including human FAPs. Using LC-MS/MS profiling, we demonstrated that LY2090314 exerts WNT mimicking properties to inhibit human FAP adipogenesis through, at least, two independent mechanisms, both mediated by β-catenin. A primary mechanism is ascribed to the role of LY2090314 in inhibiting GSK kinase, while a second indirect mechanism further strengths GSK blockage via WNT5A up regulation.

To demonstrate the clinical value of LY2090314, we established a novel method to study fat infiltrates in a three-dimensional (3D) scale. Biomimetic matrices are paving the way for the generation of affordable humanized models for medical and research applications, allowing to scale up cell-based evidence in more complex and clinically-valuable tissue-like systems

(Celikkin et al., 2021; Fernández-Garibay et al., 2022; Fuoco et al., 2012). Using the photopolymerizable Poly-Ethylene-Glycol-Fibrinogen (PF) hybrid biomimetic matrix with

FAPs, we generated a miniaturized fatty infiltrate 3D model. Employing this novel platform, we showed that a two-digit nanomolar dose of LY2090314 is effective to repress 3D adipogenesis, thus providing the proof of principle for the use this compound to limit FAP-derived fat infiltrates in diseased muscles. In addition, our miniaturized 3D fatty depot represents a scalable system to collect cellular and molecular details regarding the impact of drugs while predicting in a 3D scenario clinical outcome, unwanted side effects as well as complementary molecular targets for combinatorial anti-adipogenic therapies.

Results

A transcriptional competent β-catenin complex is the most downstream effector repressing adipogenesis

3T3-L1 cells are immortalized murine preadipocyte cells that are widely used to shed light in the molecular routes that drive the transition of preadipocytes into lipid-laden cells (Rosen and Spiegelman, 2000). Adipogenesis of this cell line is promoted by pro-differentiation hormones supplemented in the adipocyte differentiation medium (ADM): insulin, synthetic glucocorticoids, such as dexamethasone, and the phosphodiesterase inhibitor 1-methyl-3-isobutyl xanthine (IBMX) (Rosen and Spiegelman, 2000).

After three days of ADM culture, 3T3-L1 started to express canonical adipogenic markers as a sign of the activated adipogenic differentiation. Specifically, the expression of two members of the *Cebp* family (*Cebpa* and *Cebpb*) as well as the master adipogenic gene *Pparg* were significantly induced by ADM exposure (Fig.S1A). Incubation with ADM increased PPARγ protein level that exclusively localizes in the nucleus of cells undergoing adipogenesis (Fig.S1B). Time course experiment confirmed the differentiation kinetics of these cells (Fig.S1C). Specifically, PPARγ expression (used as an early adipogenic marker) was detected at the 3rd day after ADM incubation while Perilipin (that marks terminally differentiated cells) started to appear at the 5th day and progressively increased until complete maturation of 3T3-L1 cells (Fig.S1C). The phenotype conversion into adipocytes can be revealed using a highly specific dye, such as Oil Red O (ORO), highlighting mature lipid-laden cells (Fig.S1D, E). Therefore, the presented results demonstrated that 3T3-L1 cells do not spontaneously differentiate into adipocytes. Conversely, ADM incubation triggers a well-defined kinetics leading to the conversion of these progenitors into mature lipid-laden cells.

Embryonic pathways such as NOTCH, SHH and WNT/β-catenin control several aspects of adipose biology, including embryogenesis, postnatal development, induction of differentiation and homeostasis (Rosen and MacDougald, 2006). Even though this notion is well-consolidated in literature, our knowledge mostly comes from experiments that consider one of these pathways at a time. Thus, such lack of information is possibly hindering the relevance of one of these pathways compared to the others. For these reasons, we sought to identify which signaling pathway, among NOTCH, SHH and WNT/β-catenin, has a prominent role in repressing the adipogenic programs of 3T3-L1. We selected SAHM1, GANT61 and iCRT-3 to block with high selectivity the transcriptional program of NOTCH, SHH and WNT/β-catenin, respectively (Figure 1A). Briefly, SAHM1 disrupts the binding between NCID and RBPJ blocking the activation of NOTCH target genes. Similarly, iCRT-3 displaces the interaction between β-catenin and its transcriptional partner TCF/LEFs. By contrast GANT61 blocks Gli1 and Gli2 activity by aborting the SHH mediated signaling (Figure 1A). Such an approach offers the advantage to target as downstream as possible such signaling routes with a reduced interference of upstream and collateral pathways.

We tested the inhibitory effect of these small molecules in unstimulated 3T3-L1 with the aim of identifying whether a single inhibition pathway may stimulate adipogenesis in the absence of the ADM (Fig.1B). Each compound has been tested at two different doses (10 and 20 μM) in agreement with literature reports demonstrating the safety and non-cytotoxicity of these compounds (Ashley et al., 2015; Mazumdar et al., 2011; Sharma et al., 2017). We found that only the inhibition of the transcriptional activity of β-catenin by iCRT-3 is sufficient to stimulate adipogenesis in cultured 3T3-L1, in the absence of adipogenic stimuli (Figure 1B), as revealed by the fractions of ORO-positive cells (Figure 1C). This suggests that the transcriptional activity of β-catenin is solely responsible for repressing adipogenesis of 3T3-L1 preadipocytes. Combinatorial treatments of these compounds, tested at 20 μM, clearly demonstrated that only in the presence of iCRT-3 adipogenesis takes place (Figure 1D and 1E), suggesting that β-catenin is the most downstream effector repressing adipogenesis. Hence, the control of NOTCH and SHH on this phenotype is either dependent on β-catenin or dependent on an intermediate factor that in turn impairs β-catenin transcriptional activity (Figure 1F).

LY2090314 raises β-catenin concentrations and abrogates adipogenesis of 3T3-L1 and hASCs

The data collected pointed out β-catenin as a molecular determinant controlling the adipogenic differentiation of 3T3-L1 cells. Thus, we sought to investigate β-catenin dynamics during 3T3-L1 adipogenesis. To this end, we monitored the levels of β-catenin protein, during the first three days of 3T3-L1 cell differentiation. Notably, western blot analysis revealed a progressive temporal decrease of β-catenin expression during 3T3-L1 adipogenesis (Fig.S2A). Immunofluorescence analysis displayed a significant reduction in the β-catenin signal throughout the cellular compartment of these cells undergoing adipogenesis, especially in the nucleus (Fig.S2B and S2C). To prove these observations, from a biochemical point of view, we processed whole cell lysates to enrich cytoplasm and nuclear protein fractions. Three days of incubation with the ADM were sufficient to cause an almost total depletion of β-catenin from the nuclear compartment confirming the reliability of our microscopy data (Fig.S2D).

To clarify the molecular event(s) controlling the intracellular levels of β-catenin, we performed a pharmacological-based experiment to monitor β-catenin levels upon early ADM stimulation in the presence of cycloheximide, MG132 and Concanamycin A, compounds that block translation, proteosome and autophagy activities, respectively. Intriguingly, only MG132 was effective in rising β-catenin concentrations suggesting that β-catenin is subjected to a proteasome-dependent degradation (already at 24 hrs) after ADM exposure (Fig.S2E and S2F). MG132 exposure promoted the accumulation of a small band with higher molecular weight corresponding to the mono-ubiquinated form of β-catenin (Fig.S2E), an event that is consistently lost when the translation is inhibited by cycloheximide. Overall, our data demonstrated that the activation of the adipogenic program requires a decrease of the cellular concentrations of β-catenin, especially its nuclear fraction, and that such reduction is mediated by proteasome degradative processes.

To assess whether interfering with β-catenin levels, namely a decrease, may have an impact on the adipogenic fate of 3T3-L1, we focused our attention on the GSK3 kinase that is known to prime β-catenin for its degradation, via phosphorylation. To test this hypothesis, we exploited LY2090314 to stimulate β-catenin accumulation within cells (Fig.2A). LY2090314 is a highly selective GSK3 inhibitor capable to exert its action in a nanomolar concentration range, thus having a great translation potential (Atkinson et al.,

2015; Kunnimalaiyaan et al., 2018). Short-term incubation (3 days) with 20 nM of LY2090314 is sufficient to prevent β-catenin degradation while rising β-catenin amount within 3T3-L1 cells undergoing adipogenesis (Fig.2B). Moreover, we found that such stabilization parallels with the failure of PPARγ expression, making these cells incapable to engage the adipogenic program. Consistently, 3T3-L1 fails to differentiate into mature adipocytes upon LY2090314 exposure as revealed by ORO staining (Fig.2C) and by the expression of Perilipin and PPARγ at the end point of the differentiation program (Fig.2D). Remarkably, short-term exposure to LY2090314 was sufficient to sustain the total as well as the non-phospho active form (i.e., nuclear) of β-catenin in these cells, thus promoting β-catenin accumulation within the nucleus (Fig.2E).

To corroborate such data in a primary adipose progenitor cell model, we collected primary human adipose stromal cells (hASCs), a primary cell suspension that is enriched of adipose progenitors capable of differentiating into primary adipocytes. Primary hASCs were cultured and differentiated using standard protocols giving rise to highly differentiated ORO-positive adipocytes (Fig.S2G). Like 3T3-L1 cells, β-catenin demonstrated to be subjected to the same lowering kinetics also in differentiating hASCs (Fig.S2H), suggesting that β-catenin degradation hallmarks a genuine adipogenic program. Incubation with 20 nM of LY2090314 is sufficient to prevent β-catenin degradation while significantly rising the intracellular concentrations of this protein effector (Fig.S2I). Such event parallels the failure of hASCs to acquire a terminally differentiated phenotype, as revealed by the absence of ORO positive adipocytes (Fig.S2J). Contextually, PPARγ and Perilipin expression (Fig.S2K) were halted in hASCs exposed to anti-adipogenic doses of LY2090314.

To mechanistically prove that LY2090314 is acting by stabilizing a nuclear transcriptionally active complex containing β-catenin, we attempted to rescue adipogenesis in LY2090314-treated 3T3-L1 by co-exposing cells to increasing doses of iCRT-3. Incubation with iCRT-3 significantly re-sensitizes these cells to the ADM, leading to the formation of mature adipocytes. Therefore, GSK blockage by LY2090314 raises β-catenin intracellular levels and inhibits adipogenesis by stabilizing active β-catenin transcriptional complex (Fig.2F).

All together, these data indicate that adipogenesis of adipose progenitors can be modulated by altering β-catenin concentrations and that LY2090314 is highly effective in abrogating the differentiation fate of cell models endowed with adipogenic potential (Fig.2G).

LY2090314 impairs adipogenesis of primary fibro/adipogenic progenitors of murine and human origin.

Alteration of fibro/adipogenic progenitor (FAP) homeostasis is commonly found in muscle degenerative disorders. In muscular dystrophies, the myofibers breakdown coupled to an inefficient muscle regeneration leads to the progressive replacement of the contractile tissue with fat, that largely infiltrates muscle fibers. The cell origin of this non-muscle tissue has been ascribed to the altered behavior of FAPs (Giuliani et al., 2021; Theret et al., 2021). In a diseased or massively injured environment, as in the case of glycerol damage, FAPs lose their pro-regenerative role and, in this context fully experience their mesenchymal nature by differentiating into adipocytes (Stumm et al., 2018), as highlighted by the tight relation between PDGFRα (the FAP distinctive marker) cells and Perilipin depots (Fig.S3A). For this reason, FAPs are considered a good cell target for developing novel therapies aimed at limiting fatty degenerative diseases in muscular dystrophies (Kopinke et al., 2017; Reggio et al., 2020a; Reggio et al., 2020b; Zhao et al., 2020). Consistently, we previously demonstrated that once isolated from mdx dystrophic mice FAPs are prone to engage adipogenesis and that short-term exposure to LY2090314 desensitizes this detrimental fate (Reggio et al., 2020b). To confirm these findings in a more robust setup, we isolated wild-type murine FAPs (mFAPs) from 3 different C57/BL6J mice and subjected these mFAP preparations to adipogenic differentiation (Fig.S3B). Adipogenic induction stimulated the expression of the master adipogenic gene PPARγ while downregulating the expression of β-catenin (Fig.S3C). By contrast, 20 nM of LY2090314 sustained β-catenin levels and impaired PPARγ expression (Fig.S3C). Consistently, iCRT-3 increased the fraction of mFAPs-derived adipocytes in a dose-dependent manner (Fig.S3D), by inhibiting active β-catenin transcriptional complexes. Therefore, mFAPs-derived adipocytes were not present in cell cultures exposed to LY2090314 compound (Fig.S3E). Collectively these data indicate LY2090314 as a candidate agent to counteract fat infiltrates in muscular dystrophies, by halting FAP adipogenic propensity.

To formally prove the biological relevance of our model and clinical impact of this pharmacological agent, we decided to explore the impact of LY2090314 compound on human derived FAPs. To collect multidimensional information from human-derived samples, we decided to couple standard differentiation assays with state-of-the-mass spectrometry-based proteomics allowing the dissection of molecular details from human FAP cultures, at high-resolution and unbiased level.

To this end, we purified FAPs from human skeletal muscle biopsies of three healthy donors to establish primary cultures of CD56^{-}/CD15^{+} progenitors (Arrighi et al., 2015; Suárez-Calvet et al., 2021), hereafter referred to as hFAPs (Fig.3A).

Next for each donor, we exposed the resulting primary cultures to ADM either supplemented with the vehicle or with 20 nM LY2090314, for three days. Upon three days of adipogenic priming, hFAPs were harvested for proteomics (Fig.3A). In-solution (LC)-MS/MS quantitation approach allowed us to identify ~3,300 unique proteins (Table S1). Principal component analysis (PCA) revealed that the collected proteomes efficiently discriminate different samples, grouping them according to their treatment conditions (i.e., vehicle or LY2090314) (Fig.3B). LY2090314 impacts the proteome of FAPs differentiating into adipocytes: approximately the ~3% of the FAP proteome was found significantly different (FDR<0.05, fold difference>±1), allowing the identification of 71 differentially regulated proteins (31 up-regulated and 40 down-regulated) (Fig.3C).

Next, we interrogated Gene Ontology (GO) libraries to unbiasedly identify biological terms that are positively (Table S2) or negatively (Table S3) enriched by LY2090314 compound. According to their adjusted *p*-value, WNT-related terms were found to be over-represented in cultures exposed to LY2090314 (Fig.3D, full enrichment analysis is provided as Table S2), implying that the anti-adipogenic properties of this compound may be ascribed to its ability of acting as a WNT phenocopying agent. Consistently, volcano plot representation shows that β-catenin (CTNNB1) protein is significantly and massively induced by LY2090314 while the adipogenic marker FABP4 is among the most depleted proteins (Fig.3E). Consistently, short-term incubation with 20 nM LY2090314 sustained β-catenin expression and completely abrogated the ability of hFAPs to differentiate into adipocytes in the presence of ADM (Fig.3F,G). Therefore, LY2090314 represses adipogenesis by acting as a WNT surrogate in human FAPs.

Surprisingly, we found that LY2090314 also increased the protein abundance of WNT5A (Fig.3E), that we previously demonstrated to be capable, via a β-catenin-dependent mechanism, of restricting adipogenesis of murine dystrophic FAPs (Reggio et al., 2020b).

To rationalize the content of information of our proteomic survey, we mapped the 71 significantly modulated proteins (input nodes) onto a literature-derived network of signaling and physical interactions. For the purpose we used SIGNOR database through a recently developed app in the cytoscape environment. To increase the connectivity between our protein entities, we used the possibility to include "bridge" proteins via a native SIGNOR algorithm (Lo Surdo et al., 2022).

The resulting network encompasses 51 nodes including receptors, signal transducers, transcription factors and phenotypes while relationships between nodes are either positive (activations) or negative (inhibitions) (Table S4). Here, we were capable to identify a network module centered on β-catenin (Fig.S3F). Moreover, to increase the coverage of information, we also included the expression values for those protein entities that were dosed/quantified throughout this study (Fig.3H).

The subnetwork accurately describes incoming and outcoming stimuli of β-catenin while highlighting its negative relation over the adipogenic transcription factors, especially on PPARG and CEBPA. Such inhibitory role is potentiated by the upregulation of WNT5A that contributed to stabilize β-catenin by GSK3 blockage (Fig.3H).

Altogether, these data demonstrated that the anti-adipogenic role of LY2090314 is ultimately mediated by β-catenin through, at least, two independent mechanisms: a primary mechanism that is ascribed to the role of LY2090314 of inhibiting GSK kinase, and a second indirect mechanism that further strength GSK blockage role via WNT5A.

Development of a 3D adipogenic model to test LY2090314 efficacy in mitigating fatty degenerative diseases.

In our lab, we developed and optimized reliable methods for the generation of 3D organoids using muscle progenitor cells (Fuoco et al., 2015). The system is based on photopolymerizable mixture of Poly-Ethylene-Glycol (PEG) and Fibrinogen (PEG-Fibrinogen: PF) that was extensively demonstrated as (i) biocompatible and FDA-approved, (ii) suitable for 3D culture of myogenic progenitor cells (Testa et al., 2020) and (iii) adapted for the generation of mature and functional human and murine myosubstitutes that efficiently graft in host recipient muscles (Costantini et al., 2021). Starting from these notions, we tested the possibility for generating 3D models of adipogenesis by culturing adipose progenitors in a PF-based 3D microenvironment. To this end, hFAPs were resuspended in 8 mg/ml PF matrix scaffold (Fig.4A). The resulting mixture was then loaded in a polytetrafluoroethylene (PTFE) caster and polymerized by exposing the mold chamber to non-toxic and low-penetrating UV light (365nm) (Fig.4A,B). The polymerized PF 3D-construct was stable, anchored to the mold fork, with a volume approximately of 1 cm^3 and easily manipulable in classical culture vessels (Fig.4B). Suprascapular transplantation of hFAP organoids in immunodeficient mice resulted in vascularized fibro/adipose depots (Fig.4C), resembling those that can be found in some human fatty degenerative conditions. As a consequence of a spontaneous fibro/adipose differentiation

drift, cryosections of these organoids showed the presence of hFAPs that express myofibroblast and adipocyte markers such as Collagens and Perilipin, respectively (Fig.4C).

Moreover, we generated surrogate models of fat pad by using hASCs. Indeed, in this 3D culture state hASCs maintained the ability to respond to the ADM and differentiated in mature adipocytes with huge Perilipin-positive lipid droplets (Fig.4D), suggesting the suitability of this systems to generate 3D models of fat infiltrates.

LY2090314 inhibits murine and human 3D FAP adipogenesis

To this end, we tested LY2090314 at the concentration of 20 nM for its ability to inhibit 3D m/hFAP adipogenesis. In the absence of the GSK3 inhibitor, mFAPs differentiated into adipocytes as revealed by evident ORO-positive area that are visible throughout the 3D construct (Fig.5A). By contrast the incubation with 20nM LY2090314 prevented the formation of such visible ORO-positive area (Fig.5A). The longitudinal microscopy-based monitoring of these constructs clarified that LY2090314 prevented the accumulation of lipid droplets in these 3D models of fatty infiltrates (Fig.5B), as previously observed for those cells cultured in standard 2D culture vessels. Whole mount confocal microscopy demonstrated that highly mature mFAP-derived adipocytes were only observed in the absence of LY2090314 (Fig.5C). Consistently, hFAP 3D constructs failed to form highly differentiated 3D fat depots when exposed to 20 nM of LY2090314 (Fig.5D, upper and lower panel). The overall data presented in this study demonstrated that a two-digit nanomolar dose of LY2090314 compound is still effective to fully inhibit adipogenesis in a complex 3D environment, thus offering the rational proof for engaging valuable studies for testing clinical applications of LY2090314.

Discussion

Over the ruinous nature of the dystrophic damage, human muscular dystrophies are further worsened by intramuscular infiltrations of ectopic tissues, including fat, scar and occasionally mineralized tissue. As an aggravating factor, adipose infiltrates hinder the supply of nutrients to muscle fibers, limit muscle regeneration and exacerbate muscle deterioration. Non-physiological adipocytes also infiltrate the skeletal muscles of sarcopenic individuals or in obese and type II diabetes patients, contributing to the morbidity.

The origin of this deleterious fat is now ascribed to the altered differentiation behavior of fibro/adipogenic progenitors (FAPs) (Uezumi et al., 2011), a cell population that reside in the interstitial and perivascular space of the skeletal musculature(Joe et al., 2010; Santini et al., 2020). In the last ten years, several groups specialized their research in the growing field of FAP biology, elucidating roles and molecular mechanisms that helped to rationalize FAP physiology and pathogenesis, while providing concrete tools for halting or limiting their rude behavior in muscle diseases (Giuliani et al., 2021; Hogarth et al., 2019).

Hedgehog and Notch pathways have been implicated in controlling the adipogenic fate of FAPs and alterations of their signaling cascades are pointed out in FAPs from diseased muscles (Kopinke et al., 2017; Marinkovic et al., 2019).

In recent years, muscle-derived Wingless-related integration site (WNT) ligands emerge as critical niche factors capable of modulating FAP fate (Fu et al., 2022; Reggio et al., 2020b; Trensz et al., 2010). Canonical WNT3A signaling promoted the conversion of FAPs into Collagen-secreting fibroblasts (Trensz et al., 2010). Conversely, the non-canonical WNT7A has been demonstrated capable of abrogating FAP adipogenic tendency by activating the alternative WNT-RHO-YAP/TAZ signaling (Fu et al., 2022).

In addition, our group demonstrated that the reconstitution of a functional WNT5A/GSK3/β-catenin axis restricts adipogenesis of dystrophic FAPs (Reggio et al., 2020b). Remarkably, we demonstrated that WNT phenocopying agents, namely GSK3 inhibitors, may protect muscles from glycerol-induced fatty degeneration (Reggio et al., 2020b).

Therefore, these and other studies imply that, despite certain challenges, ad hoc manipulation of WNT pathway components is eligible for designing novel therapies to selectively target FAP adipogenicity.

To increase the clinical value of these observations, in the present work, we identified the β-catenin transcriptional complex as an entity that intimacy represses adipogenesis of adipose precursor cells. Contextually, we tested the potential use of GSK3 inhibitor LY2090314 as a WNT phenocopying agent that stimulates stabilization and accumulation of β-catenin. LY2090314 is a highly potent GSK3 inhibitor exerting its anti-adipogenic effect in the nanomolar range, significantly reducing promiscuous actions as well as unwanted off-target effects.

We demonstrated that the antiadipogenic effect of LY2090314 is conserved in a panel of murine and human adipose progenitor cells, including human FAPs. Therefore, this suggest that β-catenin-mediated adipogenic repression is a highly conserved mechanism that can be manipulated to control the differentiation of adipose precursors cells.

Moreover, using LC-MS/MS profiling, we uncovered that LY2090314 exerts WNT mimicking properties to inhibit human FAP adipogenesis through, at least, two independent mechanisms, both mediated by β-catenin: a primary mechanism ascribed to the role of LY2090314 of inhibiting GSK kinase, and a second indirect mechanism that further strength GSK blockage via up regulation of WNT5A.

Translating promising data in successful pre-clinical studies and/or clinical trials remains one of the hardest challenges for research that is focused on identifying novel pharmacological compounds for dystrophies treatment. Indeed, while promising, most of these data are limited to basic *in vitro* systems (i.e., 2D cultures) and fail to be verified in humanized animal models. Such drawbacks are often caused by limited testing steps in most complex culture scenarios, that would be needed to adjust doses, evaluate cellular responses and to model the clinical outcomes at cell resolution level. To overcome such limitation, we presented the possibility to generate 3D models of fat infiltrate by combining the photopolymerizable PEG-Fibrinogen biomimetic matrix with murine and human FAPs. In this 3D state, FAPs are viable and graft in host recipient mice. Most importantly, in this 3D system FAPs maintained their ability to respond to external stimuli and differentiate into adipocytes. Moreover, one of the great advantages of this ectopic surrogate is the possibility to plan a long-term culturing/live monitoring of these cells, allowing longitudinal analyses and tests. By exploiting this system, we confirmed that a single two-digit nanomolar dose of LY2090314 is still sufficient to abrogate 3D FAP adipogenesis, concretizing the possibility to use LY2090314 inhibitor to limit fatty degeneration in higher systems. The integration of our current molecular knowledge on FAPs with the development of 3D humanized disease models will help in concretizing clinical therapeutic interventions for treating secondary complication of human dystrophy.

Materials and methods

Mouse models

C57BL/6J and NOD/SCID mice were bred and maintained according to the standard facility procedures. Experiments on animals were conducted according to the rules of good animal experimentation I.A.C.U.C. N° 432 of March 12, 2006, and under Italian Health Ministry Approval No. 271/2021-PR.

Human samples

The studies involving human participants were reviewed and approved by IFO (Istituti Fisioterapici Ospitalieri, Rome) ethics committee. The patients/participants provided their written informed consent to participate in this study, in line with Helsinki Declaration. Donors were all healthy: XX53, XY65 and XX57. Biopsies have been taken during orthopedical intervention. FAPs have been isolated from muscle biopsies. ASC have been isolated from subcutaneous fat tissue.

Isolation of primary murine FAPs

FAPs were isolated from the hind limbs of male wild type C57BL/6J mice. Briefly, hind limbs were surgically removed and then minced in HBSS (GIBCO) supplemented with 100 U/ml P/S (Roche) and 0.2% BSA (AppliChem). For each mouse, the homogeneous muscle tissue preparation was enzymatically digested in 2 µg/µl collagenase A, 2.4 U/ml dispase II, and 10 µg/ml DNase I (Roche) in Dulbecco's phosphate-buffered saline (BioWest) w/calcium and magnesium. Enzymatic digestion was performed for 1 h at 37°C with gentle shaking. The homogenate underwent consecutive filtration through 100, 70, and 40 µm cell strainers (Corning). Before each filtration step, cells were centrifuged at 700g for 10 min at 4°C and then resuspended in fresh HBSS. Red blood cells were lysed in RBC lysis buffer (Santa Cruz). Freshly isolated muscle mononuclear cells were then resuspended in Magnetic beads buffer (0.5% BSA and 2 mM EDTA in 1× PBS) and filtered through a 30-µm Pre-Separation Filter (Miltenyi) to remove large particles. The whole cell suspension underwent subsequential incubations with the microbead-conjugated antibodies used for magnetic sorting. The sorting procedures and the labelling procedures with the microbead-conjugated antibodies were performed according to the manufacturer's instructions. FAPs were selected as Lin-/α7-int-/Sca-1+ cells.

Freshly sorted murine FAPs were resuspended in FAPs-GM consisting of high-glucose (25 mM) DMEM GlutaMAX supplemented with 20% FBS, 10 mM Hepes, 1 mM sodium pyruvate, and 100 U/ml P/S. After four days the FAP-GM was fully refreshed and cells cultured for two additional days before the induction of the adipogenic differentiation. Adipogenic differentiation was induced incubating FAPs with the adipocyte differentiation medium (ADM: FAPs-GM supplemented with 1 µg/ml insulin, 0.5 mM 3-isobutyl-1-methylxanthine, and 1 µM dexamethasone) for 3 d followed by two additional days in adipocyte maintenance medium (AMM: FAP-GM supplemented with 1 µg/ml insulin). Unstimulated cells were maintained in fresh FAP-GM.

Isolation of primary human FAPs

Muscle biopsies were obtained as res nullius from surgeries on healthy donors, thanks to a collaboration with Istituti Fisioterapici Ospitalieri (IFO) hospital. Muscle homogenates were subjected to in the presence of dispase, collagenase and DNase I adopting the same protocol used to release murine FAPs. The resulting suspension was filtered and plated for 10 days in Cytogrow (Resnova) to allow cell amplification. For enriching human FAPs, amplified cells were stained with microbead-conjugated antibodies and selected as CD56-/CD15+ cells. Freshly sorted human FAPs were cultured and differentiated into adipocytes by adopting the protocols tested for the murine counterpart. Notably, to enhance adipogenesis of these cells, 1 μM rosiglitazone was added to standard ADM.

Generation of a 3D model of fatty infiltration

All the experiments were performed by using PolyEthyleneGlycol-Fibrinogen (PF) biomimetic matrix. 3D fat infiltrate models were fabricated by a casting method. Briefly, PF 8mg/ml, supplemented with 0.1% of Irgacure™2959 photoinitiator solution (Ciba Specialty Chemicals) was loaded with hFAPs or mFAPs. The fork was placed in the mold and the cell-hydrogel mixture poured in a polytetrafluoroethylene (PTFE) caster. The mixture was polymerized by exposing the mold chamber to non-toxic and low-penetrating UV light, for 5 minutes. The polymerized constructs were gently removed and transferred in normal dishes containing FAP-GM and then used according to the experimental needs.

Transplantation of 3D constructs loaded with hFAPs

Two-month-old male NOD/SCID mice (n=5) were anesthetized with a 1:1 mixture of ketamine (5 mg/mL) and xylazine (1 mg/mL) at a dose of 10 mL/kg i.m. A limited skin incision on the medial side of the back has been practiced, dorsal muscle was separated from the skin, the hFAP derived construct was carefully positioned and skin closure was performed by non-absorbable 6-0 silk sutures (Clinsilk). Mice were sacrificed at 28 days after implantation for morphological analysis.

Isolation of primary hASCs

Fat biopsies were obtained as res nullius from surgeries on healthy donors, thanks to a collaboration with Istituti Fisioterapici Ospitalieri (IFO) hospital. To release hASCs, fat biopsies were digested with an enzymatic mix containing Collagenase type II for 1hr at

37°C. hASCs were cultured and differentiated using the same protocols adopted for human FAPs.

Drug compounds

All the compounds used in this study were purchased from Selleckchem and reconstituted according to manufacturer's instructions.

Glycerol injury and muscle sections preparation and labelling

For glycerol muscle injury 50 µl of 50% v/v of hypertonic solution of glycerol was administered intramuscularly into the Tibialis Anterior of C57BL/6J mice. The contralateral limb was equally injected with saline solution, as internal control. After 14 days, mice were sacrificed and the hind limb muscles were surgically removed, embedded in optimal cutting temperature and snap-frozen in liquid nitrogen. Muscle sections with 10 μM thickness were obtained using a Leica cryostat. Muscle sections were immunolabelled for PDGFRα and Perilipin expression.

Real-time PCR

Total RNA was extracted using TRIzol. Before resuspension, total RNA was precipitated overnight in the presence of 10 µg of glycogen. RNA concentration was assessed using NanoDrop Lite Spectrophotometer. Total RNA (1,000 ng) was reverse transcribed into cDNA with PrimeScript RT Reagent Kit. qPCR reactions were carried out with SYBR Premix Ex Taq (Tli RNaseH Plus) and performed in technical duplicates for each biological repeat. Each reaction mixture (final volume of 20 µl) contained 50 ng of cDNA. Actb was used as reference genes.

Immunoblot

Cells were washed in PBS 1X and lysed in ice cold lysis buffer (150 mM NaCl, 50 mM Tris-HCl pH 7.5, 1% Nonidet P-40, 1 mM EDTA, 1% Triton X-100) supplemented with 1 mM ortovanadate, 1 mM NaF, protease inhibitor mixture 1X (Sigma-Aldrich, Catalog P8340), inhibitor phosphatase mixture II 1X (Sigma-Aldrich, catalog 5726) and inhibitor phosphatase mixture III 1X (Sigma-Aldrich, catalog P0044) prior to use. Cell lysates were incubated in ice for 30 minutes and then separated at 15,500×g in a refrigerated centrifuge. Protein concentration was estimated using Bradford reagent (BioRad, catalog 500-0006). Total protein extracts were resolved by 10%, 15% SDS-PAGE or 4-20% Bio-

Rad CRITERION® gradient gel according to the needs. Proteins were transferred to Trans-Blot® Turbo mini or midi nitrocellulose membranes (Bio-Rad, catalog 1704156–1704157) using a Trans-Blot® Turbo™ transfer System (Bio-Rad) and the non-specific binding were saturated for 1 hour at room temperature (RT) in blocking solution (5% milk, 0.1% Tween-20 in 1X Tris Buffered Saline). Saturated membranes were incubated with specific primary antibodies diluted in blocking solution according to the manufacturer's instruction. The binding of primary antibodies was revealed using host-specific secondary antibodies. Chemiluminescent detection was performed using Clarity™ Western ECL Blotting Substrates (Bio-Rad, catalog 1705061) and the Fujifilm Las-3000 imaging system. Band densities were quantified using ImageJ. The brightness and contrast of each blot was adjusted using the "Auto Contrast" function in Adobe Photoshop. The full list of the antibody used is reported as TableS5.

Oil Red O
Oil Red O (Sigma-Aldrich) stock solution was prepared according to the manufacturer's instructions. Fixed cells were washed with 1× PBS and incubated for 10 min with filtered ORO working solution (3:2 ratio, ORO:ultrapure water). Stained cells were washed twice for 10 min with 1× PBS and counterstained using Hoechst 33342. ORO-stained cells were acquired via fluorescence or brightfield microscopy.

Image acquisition and analysis
Immunolabeled cells and section were acquired using the DMI6000B fluorescent microscope (Leica). Images were scored manually using Fiji by two independent collaborators in a blind analysis. Results are expressed as a ratio of the total objects counted.

Proteome sample preparation
Cells were harvested as indicated in the text and directly lysed in ice cold RIPA buffer. Proteome preparation was done using the in StageTip (iST) method (Kulak et al., 2014; Reggio et al., 2021). Samples were separated by HPLC in a single run (without pre-fractionations) and analysed by LC-MS/MS.

LC-MS/MS measurements

Instruments for LC-MS/MS analysis consisted of a NanoLC 1200 coupled via a nano-electrospray ionization source to the quadrupole-based Q Exactive HF benchtop mass spectrometer. Peptide separation was carried out according to their hydrophobicity on a home-made column, 75 um ID, 8 Um tip, 400 mm bed packed with Reprosil-PUR, C18-AQ, 1.9 um particle size, 120 Angstrom pore size (New Objective, Inc., cat. PF7508-250H363), using a binary buffer system consisting of solution A: 0.1% formic acid and B: 80% acetonitrile, 0.1% formic acid. Total flow rate: 300nl/min. LC linear gradient: after sample loading, run start at 5% buffer B for 5 min, followed by a series of linear gradients, from 5% to 30% B in 90 min, then a 10 min step to reach 50% and a 5 min step to reach 95%. This last step was maintained for 10 min.

MS spectra were acquired using 3E6 as an AGC target, a maximal injection time of 20 ms and a 120,000 resolution at 200 m/z.

The mass spectrometer operated in a data dependent Top20 mode with subsequent acquisition of higher-energy collisional dissociation (HCD) fragmentation MS/MS spectra of the top 20 most intense peaks. Resolution for MS/MS spectra was set to 15,000 at 200 m/z, AGC target to 1E5, max injection time to 20 ms and the isolation window to 1.6 Th. The intensity threshold was set at 2.0E4 and Dynamic exclusion at 30 second.

Proteome data processing

All acquired raw files were processed using MaxQuant (1.6.2.10) and the implemented Andromeda search engine. For protein assignment, spectra were correlated with the Human (v. 2021) including a list of common contaminants. Searches were performed with tryptic specifications and default settings for mass tolerances for MS and MS/MS spectra. The other parameters were set as follow: fixed modifications: carbamidomethyl (C); variable modifications: oxidation, acetyl (N-term); digestion: trypsin, Lys-C; min. peptide length = 7; max. peptide mass = 470 Da; false discovery rate for proteins and peptide-spectrum = 1%.

For further analysis, the Perseus software (1.6.2.3) (Tyanova et al., 2016) was used and first filtered for contaminants and reverse entries as well as proteins that were only identified by a modified peptide [First filter]. The LFQ Ratios were logarithmized, grouped and filtered for min.valid number (min. 3 in at least one group) [Second filter].

Missing values have been replaced by random numbers that are drawn from a normal distribution. Two - sample T-test analysis was performed using FDR = 0.05. Proteins with difference Log_2 Difference≥ ± 1 and q value <0.01 were considered significantly enriched. Categorical annotation was added in Perseus in the form of gene ontology (GO) biological process (GOBP), molecular function (GOMF), and cellular component (GOCC), and KEGG pathways.

Protein Network generation

This strategy has been previously developed and applied to query complex proteome datasets (Reggio et al., 2020a; Sacco et al., 2019)

Casual relationships between significant protein entities (coming from the LY2090314-vs-vehicle comparison) were retrieved from SIGNOR database (Lo Surdo et al., 2022)using a dedicated app in the cytoscape platform (Shannon et al., 2003). Nodes were color-coded according to their difference value (LY2090314-vs-vehicle comparison) while the dimension of nodes is proportional to their q-value.

Data availability

The mass spectrometry proteomics data have been deposited to the ProteomeXchange Consortium via the PRIDE partner repository with the dataset identifier PXD040479.

Competing interests

The authors declare that they have no conflict of interest. All authors read and approved the final version of this manuscript**.**

Bibliography

Akhmedov, D. and Berdeaux, R. (2013). The effects of obesity on skeletal muscle regeneration. *Front. Physiol.* **4 DEC**, 1–12.

Arrighi, N., Moratal, C., Clément, N., Giorgetti-Peraldi, S., Peraldi, P., Loubat, A., Kurzenne, J. Y., Dani, C., Chopard, A. and Dechesne, C. A. (2015). Characterization of adipocytes derived from fibro/adipogenic progenitors resident in human skeletal muscle. *Cell Death Dis.* **6**,.

Ashley, J. W., Ahn, J. and Hankenson, K. D. (2015). Notch signaling promotes osteoclast maturation and resorptive activity. *J. Cell. Biochem.* **116**, 2598–2609.

Atkinson, J. M., Rank, K. B., Zeng, Y., Capen, A., Yadav, V., Manro, J. R., Engler, T. A. and Chedid, M. (2015). Activating the Wnt/β-catenin pathway for the treatment of melanoma - Application of LY2090314, a Novel selective inhibitor of glycogen synthase kinase-3. *PLoS One* **10**, 1–15.

Bosnakovski, D., Chan, S. S. K., Recht, O. O., Hartweck, L. M., Gustafson, C. J., Athman, L. L., Lowe, D. A. and Kyba, M. (2017). Muscle pathology from stochastic low level DUX4 expression in an FSHD mouse model. *Nat. Commun.* **8**, 550.

Buras, E. D., Converso-Baran, K., Davis, C. S., Akama, T., Hikage, F., Michele, D. E., Brooks, S. V. and Chun, T. H. (2019). Fibro-adipogenic remodeling of the diaphragm in obesity-associated respiratory dysfunction. *Diabetes* **68**, 45–56.

Celikkin, N., Presutti, D., Maiullari, F., Fornetti, E., Agarwal, T., Paradiso, A., Volpi, M., Święszkowski, W., Bearzi, C., Barbetta, A., et al. (2021). Tackling Current Biomedical Challenges With Frontier Biofabrication and Organ-On-A-Chip Technologies. *Front. Bioeng. Biotechnol.* **9**, 1–26.

Contreras, O., Rossi, F. M. and Theret, M. (2021). Origins, Potency and Heterogeneity of Skeletal Muscle Fibro-Adipogenic Progenitors - time for new definitions. *Skelet. Muscle* **Accepted**, 1–25.

Cordani, N., Pisa, V., Pozzi, L., Sciorati, C. and Clementi, E. (2014). Nitric oxide controls fat deposition in dystrophic skeletal muscle by regulating fibro-adipogenic precursor differentiation. *Stem Cells* **32**, 874–885.

Costantini, M., Testa, S., Fornetti, E., Fuoco, C., Sanchez Riera, C., Nie, M., Bernardini, S., Rainer, A., Baldi, J., Zoccali, C., et al. (2021). Biofabricating murine and human myo-substitutes for rapid volumetric muscle loss restoration. *EMBO Mol. Med.* **13**, 1–17.

Emery, A. E. H. (2002). The muscular dystrophies. *Lancet (London, England)* **359**, 687–95.

Farup, J., Just, J., de Paoli, F., Lin, L., Jensen, J. B., Billeskov, T., Roman, I. S., Cömert, C., Møller, A. B., Madaro, L., et al. (2021). Human skeletal muscle CD90(+) fibro-adipogenic progenitors are associated with muscle degeneration in type 2 diabetic patients. *Cell Metab.* **33**, 2201-2214.e11.

Fernández-Garibay, X., Gómez-Florit, M., Domingues, R. M. A., Gomes, M. E., Fernández-Costa, J. M. and Ramón-Azcón, J. (2022). Xeno-free bioengineered human skeletal muscle tissue using human platelet lysate-based hydrogels. *Biofabrication* **14**,.

Fu, C., Guzmán-Seda, M., Laudier, D. and Han, W. M. (2022). Wnt7a Suppresses Adipogenesis of Skeletal Muscle Mesenchymal Stem Cells and Fatty Infiltration Through the Alternative Wnt-Rho-YAP/TAZ Signaling Axis. *bioRxiv*.

Fuoco, C., Salvatori, M. L., Biondo, A., Shapira-Schweitzer, K., Santoleri, S., Antonini, S., Bernardini, S., Tedesco, F. S., Cannata, S., Seliktar, D., et al. (2012). Injectable polyethylene glycol-fibrinogen hydrogel adjuvant improves survival and differentiation of transplanted mesoangioblasts in acute and chronic skeletal-muscle degeneration. *Skelet. Muscle* **2**,.

Fuoco, C., Rizzi, R., Biondo, A., Longa, E., Mascaro, A., Shapira-Schweitzer, K., Kossovar, O., Benedetti, S., Salvatori, M. L., Santoleri, S., et al. (2015). In vivo generation of a mature and functional artificial skeletal muscle . *EMBO Mol. Med.* **7**, 411–422.

Giuliani, G., Rosina, M. and Reggio, A. (2021). Signaling pathways regulating the fate of fibro/adipogenic progenitors (FAPs) in skeletal muscle regeneration and disease. *FEBS J.* **1**, febs.16080.

Hogarth, M. W., Defour, A., Lazarski, C., Gallardo, E., Manera, J. D., Partridge, T. A., Nagaraju, K. and Jaiswal, J. K. (2019). Fibroadipogenic progenitors are responsible for muscle loss in limb girdle muscular dystrophy 2B. *Nat. Commun.* **10**, 1–13.

Joe, A. W. B., Yi, L., Natarajan, A., Le Grand, F., So, L., Wang, J., Rudnicki, M. A. and Rossi, F. M. V. (2010). Muscle injury activates resident fibro/adipogenic progenitors that facilitate myogenesis. *Nat. Cell Biol.* **12**, 153–163.

Kasai, T., Nakatani, M., Ishiguro, N., Ohno, K., Yamamoto, N., Morita, M., Yamada, H., Tsuchida, K. and Uezumi, A. (2017). Promethazine Hydrochloride Inhibits Ectopic Fat Cell Formation in Skeletal Muscle. *Am. J. Pathol.* **187**, 2627–2634.

Kopinke, D., Roberson, E. C. and Reiter, J. F. (2017). Ciliary Hedgehog Signaling Restricts Injury-Induced Adipogenesis. *Cell* **170**, 340-351.e12.

Kulak, N. A., Pichler, G., Paron, I., Nagaraj, N. and Mann, M. (2014). Minimal, encapsulated proteomic-sample processing applied to copy-number estimation in eukaryotic cells. *Nat. Methods* **11**, 319–324.

Kunnimalaiyaan, S., Schwartz, V. K., Jackson, I. A., Clark Gamblin, T. and Kunnimalaiyaan, M. (2018). Antiproliferative and apoptotic effect of LY2090314, a GSK-3 inhibitor, in neuroblastoma in vitro. *BMC Cancer* **18**, 560.

Lo Surdo, P., Iannuccelli, M., Contino, S., Castagnoli, L., Licata, L., Cesareni, G. and Perfetto, L. (2022). SIGNOR 3.0, the SIGnaling network open resource 3.0: 2022 update. *Nucleic Acids Res.*

Madaro, L., Passafaro, M., Sala, D., Etxaniz, U., Lugarini, F., Proietti, D., Alfonsi, M. V., Nicoletti, C., Gatto, S., De Bardi, M., et al. (2018). Denervation-activated STAT3–IL-6 signalling in fibro-adipogenic progenitors promotes myofibres atrophy and fibrosis. *Nat. Cell Biol.* **20**, 917–927.

Marinkovic, M., Fuoco, C., Sacco, F., Cerquone Perpetuini, A., Giuliani, G., Micarelli, E., Pavlidou, T., Petrilli, L. L., Reggio, A., Riccio, F., et al. (2019). Fibro-adipogenic progenitors of dystrophic mice are insensitive to NOTCH regulation of adipogenesis. *Life Sci. Alliance* **2**, e201900437.

Mazumdar, T., DeVecchio, J., Shi, T., Jones, J., Agyeman, A. and Houghton, J. A. (2011). Hedgehog signaling drives cellular survival in human colon carcinoma cells. *Cancer Res.* **71**, 1092–1102.

Mozzetta, C., Consalvi, S., Saccone, V., Tierney, M., Diamantini, A., Mitchell, K. J., Marazzi, G., Borsellino, G., Battistini, L., Sassoon, D., et al. (2013). Fibroadipogenic progenitors mediate the ability of HDAC inhibitors to promote regeneration in dystrophic muscles of young, but not old Mdx mice. *EMBO Mol. Med.* **5**, 626–639.

Pérez-Díaz, S., Koumaiha, Z., Borok, M. J., Aurade, F., Pini, M., Periou, B., Rouault, C., Baba-Amer, Y., Clément, K., Derumeaux, G., et al. (2022). Obesity impairs skeletal muscle repair through NID-1 mediated extracellular matrix remodeling by mesenchymal progenitors. *Matrix Biol.* **112**, 90–115.

Reggio, A., Spada, F., Rosina, M., Massacci, G., Zuccotti, A., Fuoco, C., Gargioli, C., Castagnoli, L. and Cesareni, G. (2019). The immunosuppressant drug azathioprine restrains adipogenesis of muscle Fibro/Adipogenic Progenitors from dystrophic mice by affecting AKT signaling. *Sci. Rep.* **9**, 1–23.

Reggio, A., Rosina, M., Krahmer, N., Palma, A., Petrilli, L. L., Maiolatesi, G., Massacci, G., Salvatori, I., Valle, C., Testa, S., et al. (2020a). Metabolic reprogramming of fibro/adipogenic progenitors facilitates muscle regeneration. *Life Sci. Alliance* **3**, e202000646.

Reggio, A., Rosina, M., Palma, A., Cerquone Perpetuini, A., Petrilli, L. L., Gargioli, C., Fuoco, C., Micarelli, E., Giuliani, G., Cerretani, M., et al. (2020b). Adipogenesis of skeletal muscle fibro/adipogenic progenitors is affected by the WNT5a/GSK3/β-catenin axis. *Cell Death Differ.* **27**, 2921–2941.

Reggio, A., Buonomo, V., Berkane, R., Bhaskara, R. M., Tellechea, M., Peluso, I., Polishchuk, E., Di Lorenzo, G., Cirillo, C., Esposito, M., et al. (2021). Role of FAM134 paralogues in endoplasmic reticulum remodeling, ER-phagy, and Collagen quality control. *EMBO Rep.* 1–20.

Rosen, E. D. and MacDougald, O. A. (2006). Adipocyte differentiation from the inside out. *Nat. Rev. Mol. Cell Biol.* **7**, 885–896.

Rosen, E. D. and Spiegelman, B. M. (2000). Molecular regulation of adipogenesis. *Annu. Rev. Cell Dev. Biol.* **16**, 145–71.

Sacco, F., Seelig, A., Humphrey, S. J., Krahmer, N., Volta, F., Reggio, A., Marchetti, P., Gerdes, J. and Mann, M. (2019). Phosphoproteomics Reveals the GSK3-PDX1 Axis as a Key Pathogenic Signaling Node in Diabetic Islets. *Cell Metab.* **29**, 1422-1432.e3.

Santini, M. P., Malide, D., Hoffman, G., Pandey, G., D'Escamard, V., Nomura-Kitabayashi, A., Rovira, I., Kataoka, H., Ochando, J., Harvey, R. P., et al. (2020). Tissue-Resident PDGFRα+ Progenitor Cells Contribute to Fibrosis versus Healing in a Context- and Spatiotemporally Dependent Manner. *Cell Rep.* **30**, 555-570.e7.

Shannon, P., Markiel, A., Ozier, O., Baliga, N. S., Wang, J. T., Ramage, D., Amin, N., Schwikowski, B. and Ideker, T. (2003). Cytoscape: a software environment for integrated models of biomolecular interaction networks. *Genome Res.* **13**, 2498–504.

Sharma, A., Yang, W.-L., Ochani, M. and Wang, P. (2017). Mitigation of sepsis-induced inflammatory responses and organ injury through targeting Wnt/β-catenin signaling. *Sci. Rep.* **7**, 9235.

Stumm, J., Vallecillo-García, P., Vom Hofe-Schneider, S., Ollitrault, D., Schrewe, H., Economides, A. N., Marazzi, G., Sassoon, D. A. and Stricker, S. (2018). Odd skipped-related 1 (Osr1) identifies muscle-interstitial fibro-adipogenic progenitors (FAPs) activated by acute injury. *Stem Cell Res.* **32**, 8–16.

Suárez-Calvet, X., Fernández-Simón, E., Piñol-Jurado, P., Alonso-Pérez, J., Carrasco-Rozas, A., Lleixà, C., López-Fernández, S., Pons, G., Soria, L., Bigot, A., et al. (2021). Isolation of human fibroadipogenic progenitors and satellite cells from frozen muscle biopsies. *FASEB J.* **35**, 1–11.

Testa, S., Riera, C. S., Fornetti, E., Riccio, F., Fuoco, C., Bernardini, S., Baldi, J., Costantini, M., Foddai, M. L., Cannata, S., et al. (2020). Skeletal Muscle-Derived Human Mesenchymal Stem Cells: Influence of Different Culture Conditions on Proliferative and Myogenic Capabilities. *Front. Physiol.* **11**,.

Theret, M., Rossi, F. M. V. and Contreras, O. (2021). Evolving Roles of Muscle-Resident Fibro-Adipogenic Progenitors in Health, Regeneration, Neuromuscular Disorders, and Aging. *Front. Physiol.* **12**, 1–23.

Trensz, F., Haroun, S., Cloutier, A., Richter, M. V. and Grenier, G. (2010). A muscle resident cell population promotes fibrosis in hindlimb skeletal muscles of mdx mice through the Wnt canonical pathway. *Am. J. Physiol. - Cell Physiol.* **299**,.

Tyanova, S., Temu, T., Sinitcyn, P., Carlson, A., Hein, M. Y., Geiger, T., Mann, M. and Cox, J. (2016). The Perseus computational platform for comprehensive analysis of (prote)omics data. *Nat. Methods* **13**, 731–740.

Uezumi, A., Ito, T., Morikawa, D., Shimizu, N., Yoneda, T., Segawa, M., Yamaguchi, M., Ogawa, R., Matev, M. M., Miyagoe-Suzuki, Y., et al. (2011). Fibrosis and adipogenesis originate from a common mesenchymal progenitor in skeletal muscle. *J. Cell Sci.* **124**, 3654–3664.

Uezumi, A., Ikemoto-Uezumi, M. and Tsuchida, K. (2014). Roles of nonmyogenic mesenchymal progenitors in pathogenesis and regeneration of skeletal muscle. *Front. Physiol.* **5 FEB**, 1–11.

Uezumi, A., Ikemoto-Uezumi, M., Zhou, H., Kurosawa, T., Yoshimoto, Y., Nakatani, M., Hitachi, K., Yamaguchi, H., Wakatsuki, S., Araki, T., et al. (2021). Mesenchymal Bmp3b expression maintains skeletal muscle integrity and decreases in age-related sarcopenia. *J. Clin. Invest.* **131**,.

Volpi, E., Nazemi, R. and Fujita, S. (2004). Muscle tissue changes with aging. *Curr. Opin. Clin. Nutr. Metab. Care* **7**, 405–410.

Wosczyna, M. N., Konishi, C. T., Perez Carbajal, E. E., Wang, T. T., Walsh, R. A., Gan, Q., Wagner, M. W. and Rando, T. A. (2019). Mesenchymal Stromal Cells Are Required for Regeneration and Homeostatic Maintenance of Skeletal Muscle. *Cell Rep.* **27**, 2029-2035.e5.

Zhao, L., Son, J. S., Wang, B., Tian, Q., Chen, Y., Liu, X., de Avila, J. M., Zhu, M. J. and Du, M. (2020). Retinoic acid signalling in fibro/adipogenic progenitors robustly enhances muscle regeneration. *EBioMedicine* **60**, 103020.

Figures
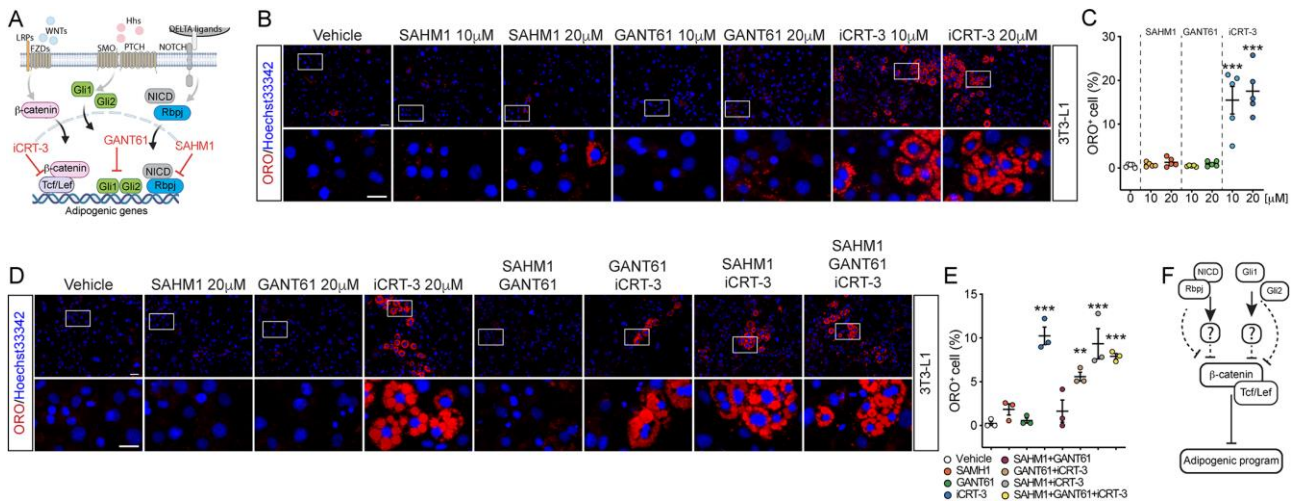
Fig. 1. A function β-catenin transcriptional complex suppresses adipogenesis of 3T3-L1 cells. (A) Schematic representation of the experimental plan. (B) Representative immunofluorescence analysis showing ORO staining after the drug perturbation experiment described in A. Cells were treated with the reported compounds for 72 hours in growth medium and then cultured for additional six days in a compound-free medium. Nuclei (blue) were revealed using Hoechst 33342. (C) Dot plot reporting the fraction of ORO-positive cells. (D) Representative immunofluorescence analysis showing ORO staining after the drug perturbation experiments with different pairwise combinations. (E) Dot plot reporting the fraction of ORO-positive cells. (F) Schematic model summarizing the results presented in figure 1. All micrographs were captured at 20× magnification. Scale bar 50 µm; inset scale bar 25 µm. Figures and data are representative of at least three independent biological repeats. The statistical significance was estimated by one-way ANOVA. All data are represented as mean ± SEM and the statistical significance is defined as **p < 0.01; ***p < 0.001.
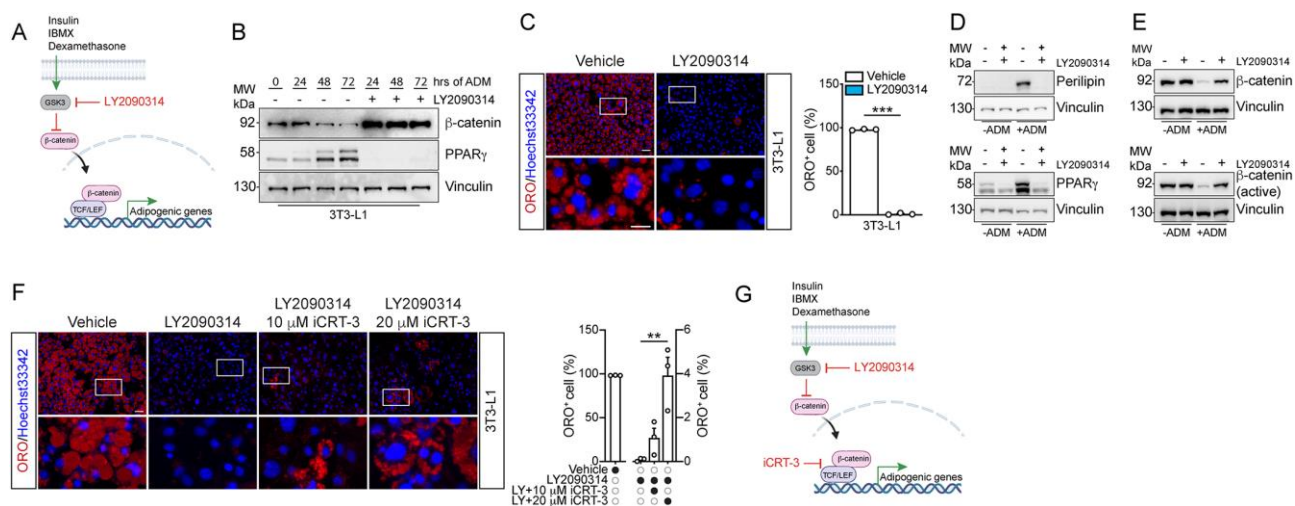
Fig. 2. LY2090314 stabilizes β-catenin intracellular amount and represses adipogenesis of 3T3-L1 cells. (A) Representative model of action of LY2090314. (B) Representative western blot showing the expression of β-catenin and PPARγ proteins during the first three days of differentiation of 3T3-L1. Vinculin is used as loading control. (C) Representative immunofluorescence showing differentiated 3T3-L1 in the presence/absence of 20nM of LY2090314. Cells were cultured for three days in ADM in the presence/absence of LY2090314 and then cultured for six additional days in a compound-free maintenance medium. Nuclei (blue) were revealed using Hoechst 33342. The associated bar plot reports the percentage of ORO-positive cells (red) in both conditions. (D) Representative western blots showing the expression of Perilipin and PPARγ proteins at the end of 3T3-L1, exposed or not to 20 nM of LY2090314. Vinculin is used as loading control. (E) Representative western blots showing the expression of β-catenin and non-phospho active β-catenin proteins at the end of 3T3-L1, exposed or not to 20 nM of LY2090314. Vinculin is used as loading control. (F) Representative immunofluorescence showing differentiated 3T3-L1 in the presence/absence of a combinatorial treatment of 20nM of LY2090314 and 10, 20 μM of iCRT-3. Nuclei (blue) were revealed using Hoechst 33342. Bar plot reporting the percentage of ORO-positive cells (red) in all the considered conditions. (G) Schematic model summarizing mechanistic details of LY2090314 and iCRT-3 in the adipogenic pathway. All micrographs were captured at 20× magnification. Scale bar 50 μm; inset scale bar 25 μm. The statistical significance was estimated by student *t*-test and one-way ANOVA, according to the group of study. Figures and data are representative of at least three independent biological repeats. All data are represented as mean ± SEM and the statistical significance is defined as **p < 0.01; ***p < 0.001.
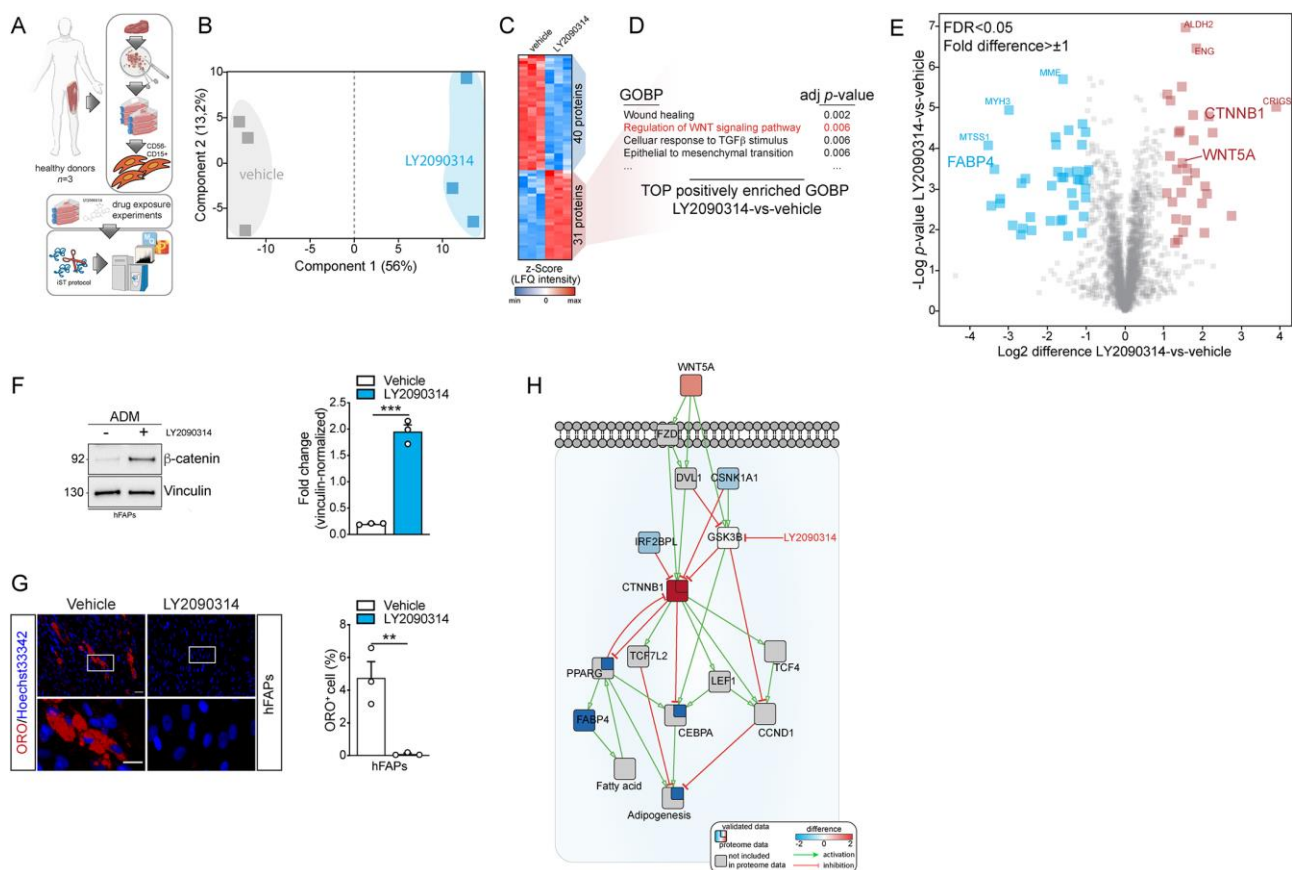
Fig. 3. LY2090314 abrogates adipogenesis of murine and human FAPs. (A) Representative scheme showing collection and utilization of human-derived FAPs (hFAPs) (B) Principal component analysis (PCA) showing sample segregation of hFAP proteomes upon exposure to LY2090314 or vehicle. (C) Heat-map showing significantly (FDR<0.05, FC>+/-1) regulated proteins in the LY2090314-vs-vehicle comparison. (D) Gene Ontology terms that are positively enriched (adj p-value<0.01) in the LY2090314-vs-vehicle comparison. (E) Volcano plot showing positively and negatively enriched proteins in the LY2090314-vs-vehicle comparison. (F) Representative western blot showing the expression of β-catenin in human FAPs in the absence/presence of 20 nM LY2090314. The bar plot reports the densitometric values of β-catenin in both conditions. (G) Representative immunofluorescence showing differentiated human FAPs (hFAPs) in the presence/absence of 20nM of LY2090314. Cells were cultured for three days in ADM in the presence/absence of LY2090314 and then cultured for six additional days in a compound-free maintenance medium. Nuclei (blue) were revealed using Hoechst 33342. The associated bar plot reports the percentage of ORO-positive cells in both conditions.

(H) Network reporting the mode of action of LY2090314 in repressing the adipogenic program of hFAPs. The statistical significance was estimated by student *t*-test. Figures and data are representative of at least three independent biological repeats. All data are represented as mean ± SEM and the statistical significance is defined as ***p < 0.001.
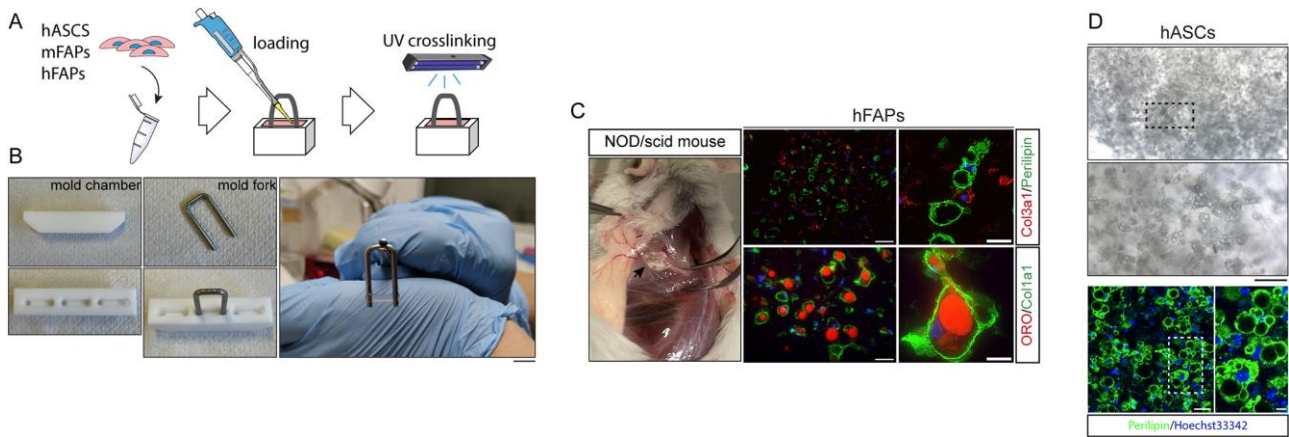
**Fig. 4**. **LY2090314 suppresses 3D adipogenesis of murine and human FAPs**. (A) Representative scheme showing the generation of a miniaturized 3D model of fat infiltration using PF hydrogel. (B) Components (i.e. the mold chamber and fork) for the generation of 3D model of fat infiltration using PF hydrogel. A representative polymerized PF construct is also shown. Scale bar: 1 cm. (C) A previously transplanted PF construct, containing human FAPs was explanted after 30 days. Representative cryosections of the explanted construct showing hFAPs expressing Col3a1 (red) and perilipin (green) (upper panel) and Col1a1 (green) and ORO (red) (lower panel). Scale bar 50 μm; inset scale bar 25 μm. (D) PF hydrogel construct loaded with hASCs induced to differentiate into adipocytes using standard protocols. 3D differentiated adipocytes with evident lipid droplets are evident in brightfield microscopy. Scale bar: 100 μm, inset is an enlarged view. Representative whole mount immunofluorescence showing perilipin expression (green) in differentiated hASCs-derived adipocytes. Scale bar: 50 μm, inset 10 μm
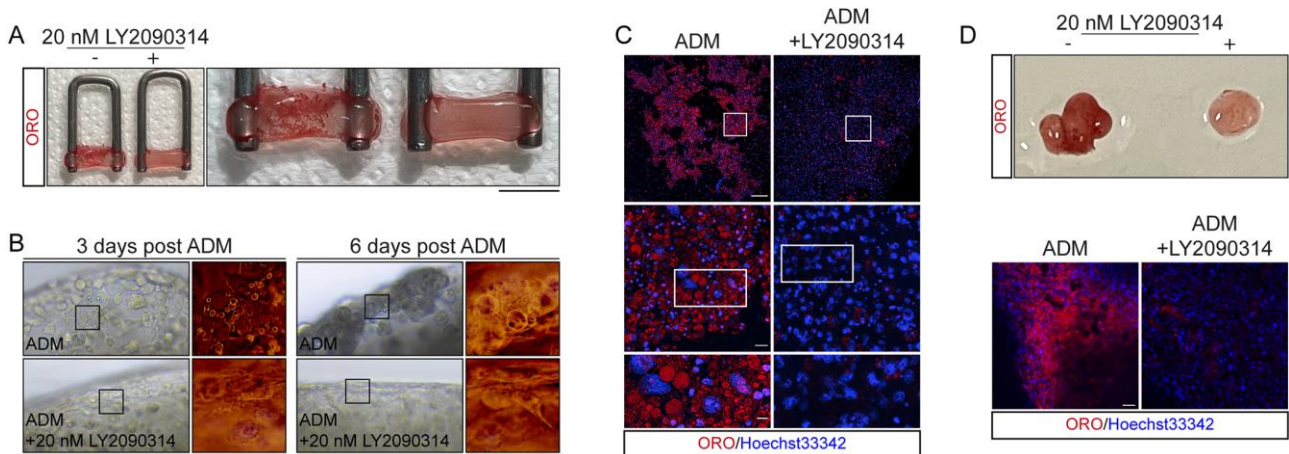
Fig. 5. LY2090314 inhibits murine and human 3D FAP adipogenesis. (A) Representative ORO staining of PF constructs previously loaded with murine FAPs. Both constructs were exposed to ADM in the absence/presence of 20 nM LY2090314. Scale bar: 1 cm (B) Representative brightfield micrographs showing mFAPs undergoing adipogenesis in the absence/presence of 20 nM of LY2090314, at 3 and 6 days after ADM exposure. Scale bar insets: 15 μM. (C) Representative whole mount immunofluorescence showing ORO labelling in mFAPs derived-adipocytes (red) differentiated in the absence/presence of 20 nM of LY2090314. Scale bar: upper panel 100 μm, middle panel 50 μm, bottom panel 10 μm. (D) Representative ORO staining of PF constructs previously loaded with hFAPs (upper panel). Scale bar: 0.3 cm. Representative whole mount immunofluorescence showing ORO labelling in hFAPs derived-adipocytes (red) differentiated in the absence/presence of 20 nM of LY2090314. Scale bar: 50 μm. Figures and data are representative of at least three independent biological repeats.
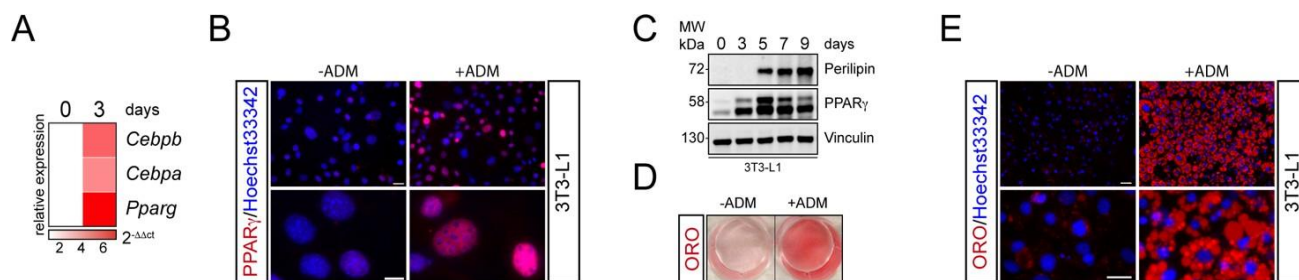
Fig. S1. (A) Heat map showing the differential gene expression of Cebpb, Cebpa and Pparg, between unstimulated and ADM-induced 3T3-L1 cells. Representative immunofluorescence showing PPARγ expression and localization in 3T3-L1 cells cultured either in growth medium or in ADM for three days. (C) Representative western blot showing Perilipin and PPARγ expression in 3T3-L1 undergoing adipogenic differentiation. Vinculin serves as loading control. (D) Representative ORO staining in 3T3-L1 cells in the presence of vehicle or ADM. (E) Representative immunofluorescence showing ORO staining in 3T3-L1 cells stimulated with the vehicle or ADM. Nuclei (blue) were labelled with Hoechst 33342. All micrographs were captured at 20× magnification. Scale bar: 50 μm; Scale bars of insets: 10 μm. Figures and data are representative of at least three independent biological repeats.
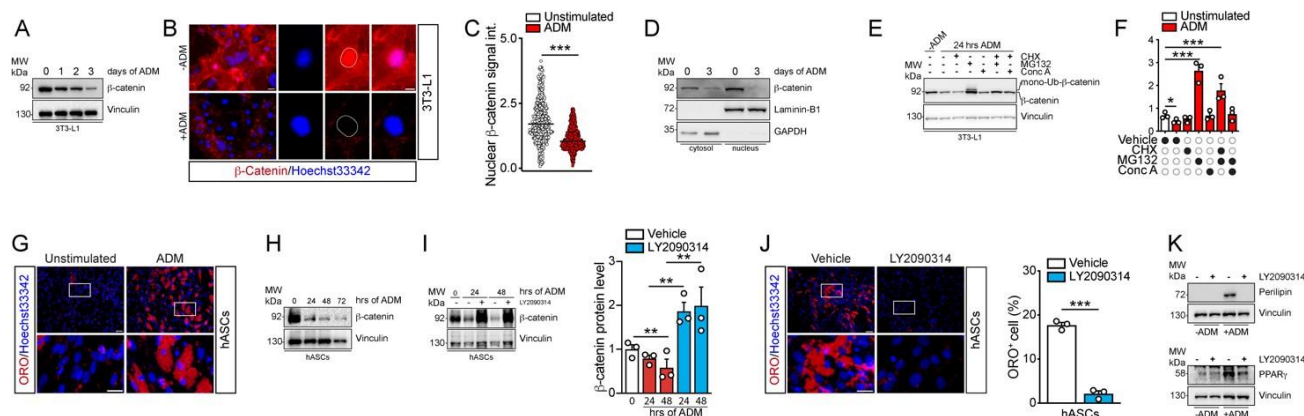
Fig. S2. (A) Representative western blot showing β-catenin expression in 3T3-L1 during the first three days of differentiation. Vinculin serves as loading control. (B) Representative immunofluorescence showing β-catenin expression and localization in 3T3-L1 cells cultured either in growth medium or in ADM for three days. Nuclei (blue) were labelled with Hoechst 33342. (C) Dot plot showing the relative quantification of the nuclear β-catenin signal in 3T3-L1 cells cultured either in growth medium or in ADM for three days. (D) Representative western blot showing β-catenin expression in cytoplasmic and nuclear enriched fractions collected from 3T3-L1 undergoing adipogenesis. (E) Representative western blot showing β-catenin expression in 3T3-L1 exposed to cycloheximide, MG132 and Concanamycin A, after 24 hours of ADM. Vinculin serves as loading control. (F) Bar plot reporting the relative quantification of β-catenin expression levels.

(G) Representative immunofluorescence showing ORO staining in hASCs exposed or not to ADM. Nuclei (blue) were labelled with Hoechst 33342. (H) Representative western blot showing β-catenin expression in hASCs during the first three days of differentiation. Vinculin serves as loading control. (I) Representative western blot showing the expression of β- catenin proteins during the first three days of differentiation of hASCs. Differentiating cells were incubated in the presence/absence of 20 nM of LY2090314. Vinculin serves as loading control. Associated bar plot reporting the relative quantification of the β-catenin expression. (J) Representative immunofluorescence showing ORO staining in hASCs exposed or not to 20 nM of LY2090314. Nuclei (blue) were labelled with Hoechst 33342. Relative bar plot reporting the fraction of ORO-positive cells in both conditions. (K) Representative immunoblots showing Perilipin and PPARγ expression in hASCs differentiated in the presence/absence of 20 nM of LY2090314. Vinculin serves as loading control. All micrographs were captured at 20× magnification. Scale bar: 50 μm; Scale bars of insets: 10 μm. Figures and data are representative of at least three independent biological repeats.
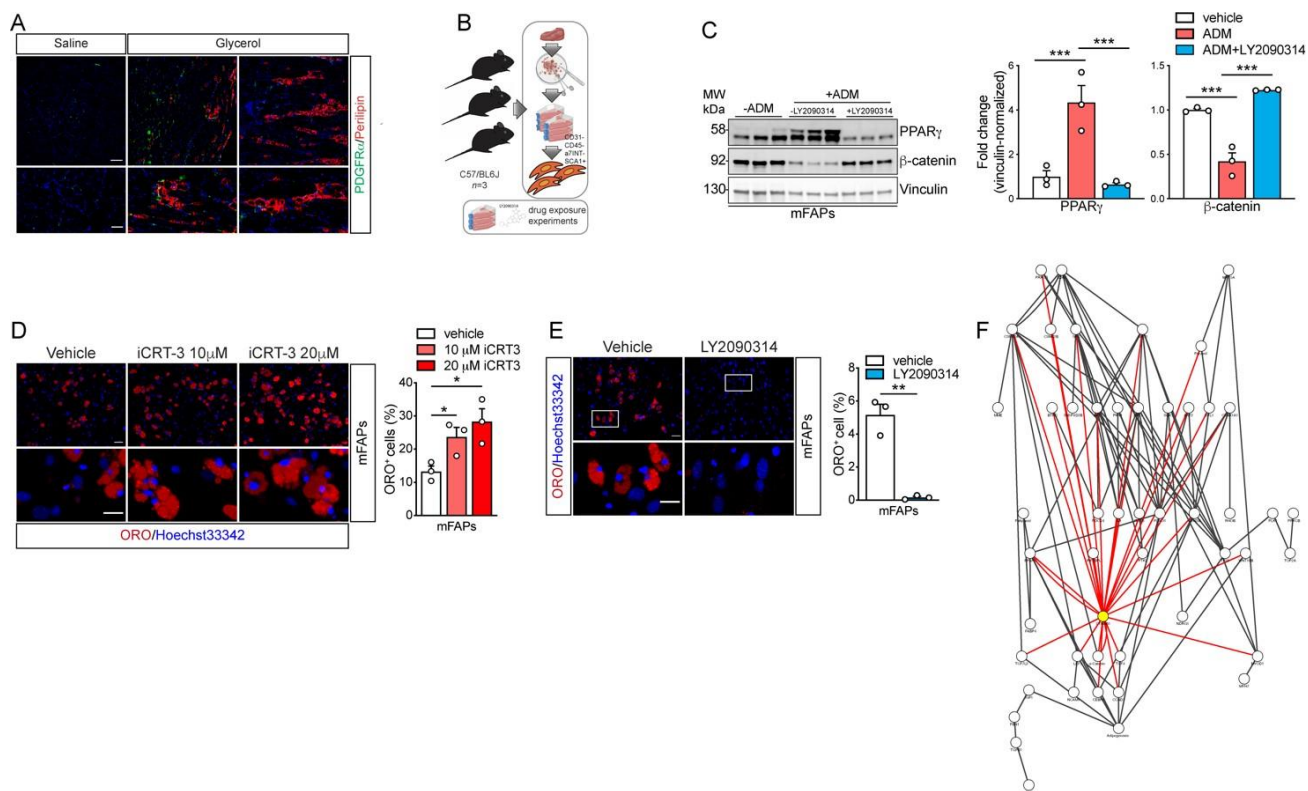
Fig. S3. (A) Representative immunofluorescence showing tibialis anterior muscle sections stained for the expression of Perilipin and PDGFRa. Tibialis anterior muscles were either injected with saline solution or with 50 ml of 50% v/v of glycerol solution. Muscles were sampled after 14 days. (B) Representative scheme showing collection and utilization of murine- derived FAPs (mFAPs). (C) Representative western blot showing the expression of b-catenin and PPARg proteins during the first three days of differentiation of 3T3-L1, in the absence/presence of 20 nM LY2090314. Vinculin is used as loading control. The bar plot reports the densitometric values of b-catenin in both conditions. (D) Representative immunofluorescence analysis showing ORO staining in differentiated mFAPs after the exposure to increasing doses of iCRT-3 (10 and 20 μM). Nuclei (blue) were revealed using Hoechst 33342. (E) Representative ORO staining showing differentiated murine FAPs (mFAPs) in the presence/absence of 20nM of LY2090314. Nuclei (blue) were revealed using Hoechst 33342. The associated bar plot reports the percentage of ORO-positive cells in both conditions. (F) Network showing the connectivity between significant and "bridge" proteins to adipogenesis. CTNNB1 is highlighted in yellow while incoming and outcoming stimuli are reported in red.

Table S1. Full table reporting proteins profiled via high-resolution mass spectrometry.

Click here to download Table S1

Table S2. List of GO terms that are positively enriched in the LY2090314-vs-vehicle comparison.

Click here to download Table S2

Table S3. List of GO terms that are negatively enriched in the LY2090314-vs-vehicle comparison.

Click here to download Table S3

Table S4. Casual interactions between protein entities that are part of LY2090314-specific network.

Click here to download Table S4

Table S5. Reagents used in this study.

Click here to download Table S5